This is our main result for the model and is plotted in Figure 2. It has in it the essential features of wave compression, wave amplification and energy storage in the USWM, as stated above. It clearly shows the competition between the loss ($1/\tau$) and the group velocity dispersion (η). Note the power-law divergence co-existing with the delta-function condensation (pile-up) of the wave intensity at the point of accumulation $x = \Delta$.

The intensity peaking (which in fact happens to be an integrable singularity for the above model choice of $\eta(x)$) is important to our phenomenological interpretation of any experiment on light storage in a USWM.

It is to be noted, however, that in the limit of $\tau \to \infty$ (that is, for no dissipation) and with a finite incoming optical pulse, the light wave simply piles up to a complete stop at $x = \Delta$. This should be the case for a USWM as realized in a Bose–Einstein Condensation (BEC)[1], and will manifest as a bright spot appearing at the point of stoppage $x = \Delta$.

It is important to emphasize here that the above phenomena of wave compression, intensity growth and energy storage are generic to any USWM. One may note in passing that this phenomenon of wave compression and amplification is, of course, analogous to that of breaking of waves at the seashore: as the wave train approaches the shore, the leading edge (being in shallower waters) advances slower relative to its trailing edge, resulting in wave compression. This in turn leads to amplitude growth or a pile-up of the compressed wave, and then to its eventual breaking close to the shoreline. The seashore acts as the slow wave medium here.

The above analytical treatment is, of course, readily generalized to the case of an arbitrary group velocity profile other than the one shown in Figure 1. This may include, in particular, the case where the point of accumulation (complete stoppage) gets replaced by a broad maximum, allowing the transmission of light beyond the peak.

In conclusion, we have proposed and solved analytically a model for light propagation in USWM having a point of accumulation where the group velocity becomes extremely low, or even vanishes. Our solution explicitly displays wave compression (pile-up), optical energy storage and a point of accumulation that characterize the USWM.

1. Dutton, Z., Ginsberg, N. S., Slowe, C. and Hau, L. V., The art of taming light: ultra-slow and stopped light. *Europhys. News*, 2004, **35**, 33–39.
2. Hau, L. V., Harris, S. E., Dutton, Z. and Behroozi, C. H., Light speed reduction to 17 metres per second in an ultracold atomic gas. *Nature*, 1999, **397**, 594–598.
3. Bigelow, M. S., Lepeshkin, N. N. and Boyd, R. W., Superluminal and slow light propagation in a room-temperature solid. *Science*, 2003, **301**, 200–202.
4. Liu, C., Dutton, Z., Berhoozi, C. H. and Hau, L. V., Observation of coherent optical information storage in an atomic medium using halted light pulses. *Nature*, 2001, **409**, 490–493.
5. Philips, D. F., Fleischhauer, A., Mair, A., Walsworth, R. L. and Lukin, M. D., Storage of light in atomic vapor. *Phys. Rev. Lett.*, 2001, **86**, 783–786.
6. Kasapi, A., Jain, M., Yin, G. Y. and Harris, S. E., Electromagnetically induced transparency: propagation dynamics. *Phys. Rev. Lett.*, 1995, **74**, 2447–2450.
7. Milonni, P. W., Fast light, slow light and left-handed light. In *IOP Series Optics and Optoelectronics* (eds Brown, R. G. W. and Pike, E. R.), Taylor & Francis, New York, 2005.

ACKNOWLEDGEMENTS. V.R. thanks Prof. Anil Kumar, IISc, Bangalore and acknowledges DST-0955 project (CQIQC) at IISc for support. He also thanks RRI, Bangalore for its hospitality during the course of this work.

Received 27 May 2013; accepted 5 September 2013

Prediction of Indian summer monsoon rainfall using surface temperature and sea-level pressure cluster parameters

S. B. Kakade* and A. Kulkarni

Indian Institute of Tropical Meteorology, Pune 411 008, India

The scientific community has been putting in continuous efforts to improve long-range forecast of Indian summer monsoon rainfall (ISMR). In this study we try to search for new predictors which may improve the prediction of ISMR. The shared nearest neighbour technique has been applied to surface temperature (ST) and sea-level pressure (SLP) to obtain the clusters in pre-monsoon months (January through May) and seasons (winter, spring). The powers of time series averaged over the clusters are used as parameters for predicting ISMR. Instead of a single prediction equation, two separate equations are developed based on the positive and negative phase of effective strength index (ESI) tendency. Simple multiple regression equations are developed using these cluster parameters for predicting ISMR during the contrasting phases of ESI tendency. During positive (negative) phase of ESI tendency, the SLP (ST) cluster parameters can predict ISMR. The prediction of ISMR is improved if we use the prediction equation depending upon the phase of ESI tendency.

Keywords: Cluster parameters, effective strength index, rainfall prediction, sea-level pressure, surface temperature.

INDIA being an agrarian country, the survival of its people mainly depends on the monsoon rains received during the

*For correspondence. (e-mail: kakade@tropmet.res.in)

four-month period from June through September. It has been observed that there is a substantial loss in agricultural output during severe droughts. There is also significant reduction in gross domestic product (GDP) during the drought years[1]. The scientific community has been trying hard to improve the long-range forecast (LRF) of Indian summer monsoon rainfall (ISMR). The correct forecasting of Indian monsoon rainfall is important for agricultural and economic planning. The prediction of ISMR has a long history and most of the studies are primarily based on statistical and empirical techniques. These studies have brought out several predictors for the ISMR. These parameters represent various forcings on the monsoon circulation system. Many earlier studies have found parameters based on surface temperature (ST) and sea-level pressure (SLP) for predicting ISMR. The northern hemisphere winter (January and February) surface air temperature anomaly was identified as an important predictor[2]. A predictor based on minimum temperatures in May over the western Indian region has also been developed[3]. Three minimum temperature parameters over northern, central and eastern coastal areas of India have also been used as predictors[4]. It has been shown that the mean ST at six stations (Jodhpur, Ahmedabad, Mumbai, Indore, Sagar and Akola) during spring season (March–May) exhibited high correlation with subsequent ISMR[5]. A predictor parameter by averaging spring-time SLP at these six stations has been developed[5,6]. Two predictors have been identified based on the minimum temperatures during March over east peninsular India and during May over west central India[7]. Many recent studies[8–13] have demonstrated the relationship between surface pressure/temperature over Eurasia and ISMR. ISMR–sea-surface temperature (SST) relationship from three seasons to four years lag prior to monsoon seasons has been used for developing prediction equations[14]. SST-based multimodel ensemble probabilistic forecast has also been made[15]. In all these studies, LRF parameters are obtained by first correlating the parameter field with ISMR and then averaging temperature/pressure field over the region of significant correlations.

In the present study we first obtain the clusters of ST and SLP during pre-monsoon months and seasons using the method of shared nearest neighbour (SNN). The technique was first developed to find the clusters in high-dimensional data[16]. It has been applied to ocean temperatures and the clusters have been used to predict land temperatures[17]. An attempt has been made here to understand the temporal and spatial variability of ST and SLP in these cluster regions. It has been demonstrated that temperature evolution from winter to spring changes with phase of effective strength index (ESI) tendency[18,19]. Hence the relationship between the averaged ST and SLP over the respective cluster regions and ISMR is studied during the contrasting phases of ESI tendency. The highly correlated clusters are considered as parameters in multiple regression equations to predict ISMR. The performance of these regression equations is also discussed.

The following data for the period 1951–2007 have been used in this analysis:

(1) The time series of ISMR (June–September) have been taken from the website of the Indian Institute of Tropical Meteorology, Pune (www.tropmet.res.in). The percentage departure from long-term mean is calculated and these indices are used in further analysis.
(2) The gridded 2.5° × 2.5° lat./long. global ST and SLP data have been taken from NCEP/NCAR reanalysis dataset. The data have been interpolated on 5° × 5° lat./long. to apply SNN algorithm.
(3) North Atlantic Oscillation (NAO) and Southern Oscillation (SO) data have been taken from www.cpc.ncep.noaa.gov.
(4) ESI is defined as the algebraic difference between monthly indices of NAO and SO. The anomalies from the annual mean have been calculated for each month and these anomaly series are then divided by the standard deviation. These series are called the ESI series of the respective months. ESI tendency is the difference between April and January ESI values.

Winter (December–February) and spring (March–May) time series are obtained by averaging the corresponding meteorological parameter values.

In order to find the parameters based on ST and SLP, we need to know the regions showing clustering of these meteorological parameters. Cluster analysis classified the data points into useful or meaningful groups. Clustering critically depends upon density and distance (similarity), but these concepts become more difficult to define as dimensionality increases. For high-dimensional data, a similarity measure has been used[16]. This is based on the number of neighbours that two points share and then density of a point is defined as the sum of the similarities of a point's nearest neighbours. The algorithm based on these ideas eliminates noise (low-density points) and builds clusters by associating non-noise points with representative or core points (high-density points). This approach handles many problems like finding clusters in the presence of noise and outliers, finding clusters in data that have clusters of different shapes, sizes and density, etc.

In SNN, similarity is confirmed by the common nearest neighbours. If point A is close to point B and if both of them are close to a set of points C, then we can say that A and B are close with greater confidence since their similarity is confirmed by the points in set C (ref. 20).

The steps involved in the SNN clustering algorithms are:

(1) To compute the similarity matrix. The correlation coefficient (CC) or the Euclidean distance between

the time series over two grid points is the typical measure of similarity.

(2) To sparsify the similarity matrix by keeping only its k strongest links. Here k is called the neighbourhood list size. It is the most important factor as it adjusts the focus of the clusters. If k is too small, even a uniform cluster will be broken up into pieces due to local variations in the similarity, and the algorithm will tend to find many small, but tight clusters. On the other hand, if k is too large, then the algorithm will tend to find only a few large, well-separated clusters and small local variations in similarity will not have an impact. In the SNN, a point can be similar to at most k other points.

(3) To construct the SNN list from the sparsified similarity matrix. At this point, we could apply a similarity threshold and find the connected components to obtain the clusters (Jarvis–Patrick algorithm.)

(4) To find the SNN density of each point. Here we consider the sum of link strengths for every point in the SNN graph. The points having high total link strength will become candidates for representative points, while those having very low total link strength become candidates for noise points.

(5) To find the core points. These are the points having SNN density greater than the threshold value. This value is to be decided by trial and error. (Here we have taken it to be 75.)

(6) To form clusters from the core points by averaging the grids in the cluster.

The SNN clustering technique has been applied[16] to monthly SLP data over 2.5° × 2.5° lat./long. from 1950 to 1994. Using these clusters the researchers[16] have been able to reproduce NAO and SO indices. The performance of SST and SLP cluster-based indices have been compared[17] with respect to known climate indices like NAO and SO. We have used the same SNN clustering method to obtain ST and SLP clusters in pre-monsoon months and seasons. For this we have used 5° × 5° grid data for 1951–2007. Generally in earth sciences CC is used as the measure of similarity between two grid points.

The CCs between ST/SLP of each grid point with all other grid points is computed for the period 1951–2007. The set of grid points showing significant CC (at 1% level) with a particular grid point forms the nearest neighbour list for that grid point. Such nearest neighbour lists are found for each grid point. For any two grid points P and Q, the common grid points in the nearest neighbour list of P and Q form the closest nearest neighbour list. These closest nearest neighbour lists at a particular grid point are arranged in decreasing order of their cardinality number. A link is created between points P and Q if and only if both P and Q have each other in their closest k nearest neighbour lists, where k is the nearest neighbour size (here k = 100).

Let i, j be two points. Then strength of the link between i and j is calculated as

$$\mathrm{Str}(i, j) = \sum (k+1-m)\times(k+1-n),$$

where k is the nearest neighbour list size, and m and n are positions of SNNs in the list of i and j. The strength at each grid point is computed using this formula. The grid points having strength greater than 75 are called as core points and then clusters are built around these core points.

Figures 1 and 2 show SLP and ST cluster regions respectively. There are 62 ST and SLP cluster regions in all pre-monsoon months and seasons. Averaged ST and SLP time series over corresponding cluster regions are prepared. In order to understand nonlinear impact of these cluster time series, CC between ISMR and different powers of cluster time series (index series) is computed. The index series showing significant CC at 5% level of significance is considered as the parameter for predicting ISMR. Table 1 describes five cluster parameters (CP1, CP2, CP3, CP4 and CP5) showing significant association

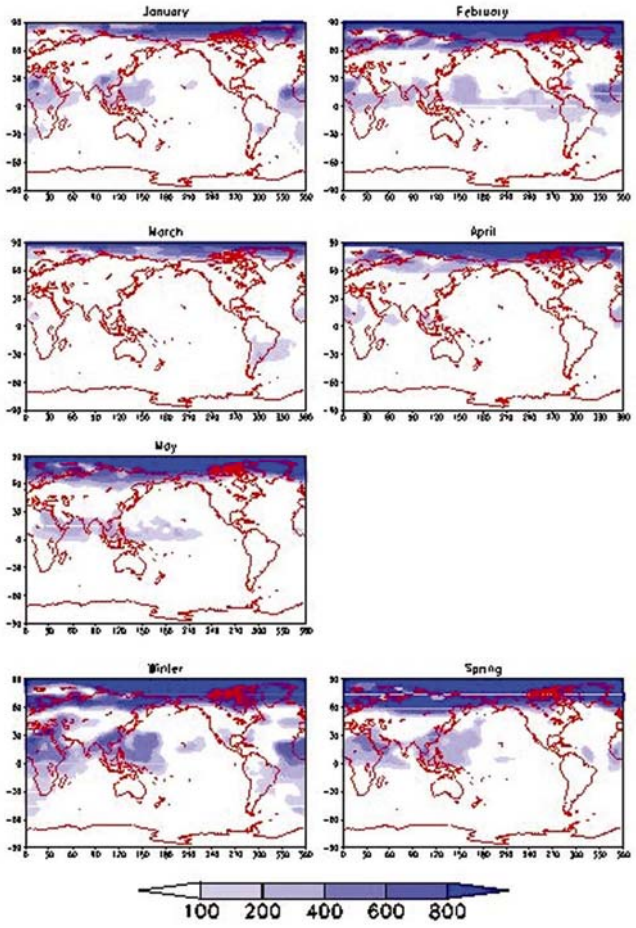

Figure 1. Sea-level pressure clusters during pre-monsoon months and seasons.

Table 1. Cluster parameters for predicting ISMR

Abbreviation	Correlation coefficient	Description
CP1	–0.35	May sea-level pressure anomaly over (Equator – 20N; 100–115E)
CP2	0.33	Cube of January temperature anomaly over (20–30N; 5–35E)
CP3	–0.31	Fifth power of spring sea-level pressure anomaly over (Equator – 40N; 85–180E)
CP4	–0.31	Cube of April sea-level pressure anomaly over (Equator – 20N; 100–140E)
CP5	–0.29	Square of winter sea-level pressure anomaly over (40–50N; 35–5W)

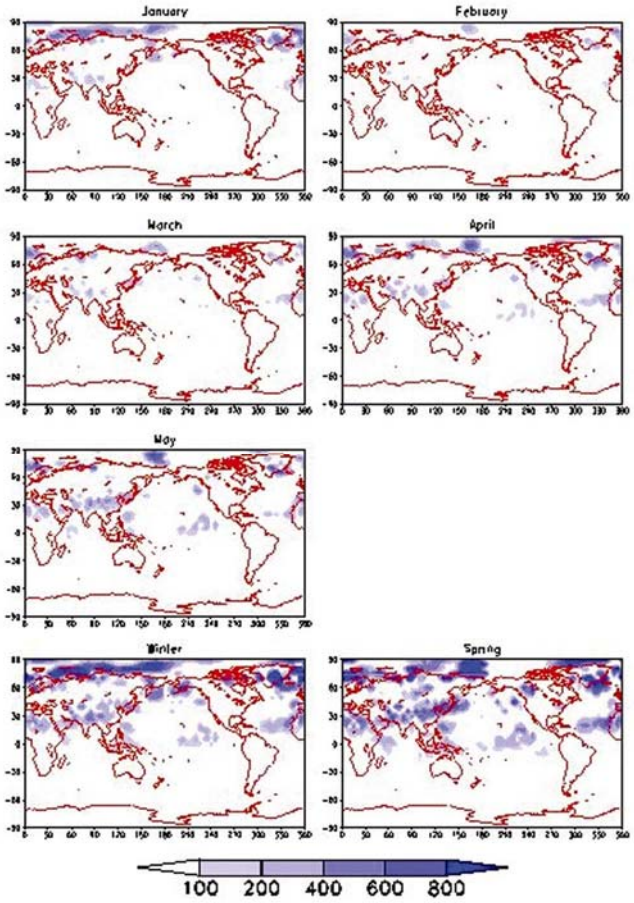

Figure 2. Surface temperature clusters during pre-monsoon months and seasons.

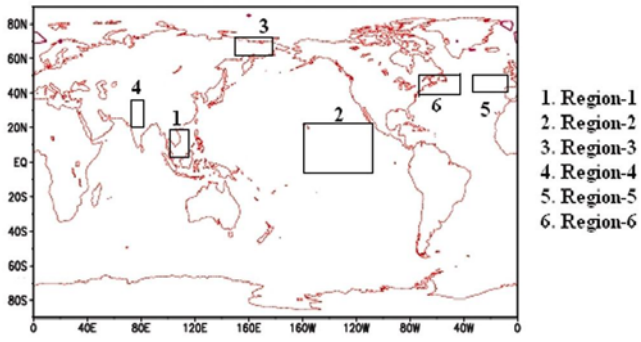

Figure 3. Locations of surface temperature/pressure cluster parameters used for predicting ISMR.

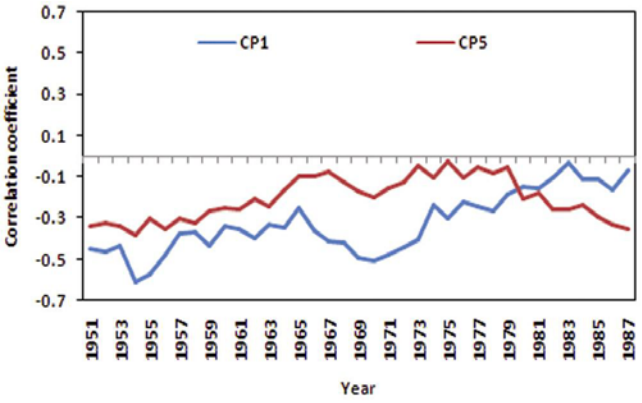

Figure 4. The 21-year sliding correlation coefficients between cluster parameters and ISMR.

with ISMR. In order to formulate a multiple regression equation, we have found out other independent parameters by computing CC among these cluster parameters. CP1 shows insignificant CC with CP5. The locations of CP1 and CP5 are depicted in Figure 3 by region-1 and region-5 respectively. The CP1 (CC = –0.35) and CP5 (CC = –0.29) are inversely associated with ISMR and the relationship is significant at 5% level. The stability of relationship between ISMR and these cluster parameters is checked by computing 21-year sliding CC between ISMR and the respective cluster parameters. Figure 4 shows 21-year sliding CC between ISMR and two cluster parameters. The probable physical explanation for this inverse relationship may be as follows: Region-1 is to the west of the Pacific Ocean and below-normal May SLP over this region can increase the number of remittances in the Bay of Bengal, which may increase the seasonal rainfall amount over India. Similarly, region-5 is influenced by Azores High in North Atlantic Ocean, which is one of the centres of action in the atmospheric oscillation (NAO). Winter SLP over this region does not show significant relationship with ISMR but has a nonlinear relationship with it, since the square of this parameter shows significant inverse association with ISMR (CC = –0.29). Below-normal winter SLP over this region is linked with negative NAO, which drives weaker westerlies carrying warm maritime air over Eurasia. Hence winter-time snow depth over western Eurasia may increase, which may be conducive for good monsoon activity over India[21].

Table 2. Cluster parameters for predicting ISMR during positive effective strength index (ESI) tendency

Abbreviation	Correlation coefficient	Description
CPP1	–0.66	Fourth power of winter sea-level pressure anomaly over (40–50N; 70–40W)
CPP2	–0.41	Square of winter sea-level pressure anomaly over (40–50N; 35–5W)
CPP3	–0.40	Fourth power of May temperature anomaly over (60–75N; 50–15W)

Table 3. Cluster parameters for predicting ISMR during negative ESI tendency

Abbreviation	Correlation coefficient	Description
CPN1	–0.57	Spring temperature anomaly over (5S–20N; 160–110W)
CPN2	0.49	Square of April sea-level pressure anomaly over (Equator – 20N; 0–30E)
CPN3	0.49	Fourth power of April sea-level pressure anomaly over (Equator – 20N; 0–30E)
CPN4	–0.48	May sea-level pressure anomaly over (Equator – 40N; 0–80E)
CPN5	0.46	Winter temperature anomaly over (20–35N; 60–70E)
CPN6	–0.46	Fourth power of spring temperature anomaly over (20–40N; 45–160E)
CPN7	–0.44	Winter temperature anomaly over (Equator – 20N; 160–110W)
CPN8	0.43	Square of spring sea-level pressure anomaly over (Equator – 40N; 0–80E)
CPN9	–0.42	Square of January temperature anomaly over (60–70N; 150–180E)
CPN10	0.42	Cube of winter temperature anomaly over (10–45N; 0–30E)
CPN11	0.41	January temperature anomaly over (50–90N; 45–5W)
CPN12	–0.40	May sea-level pressure anomaly over (Equator – 20N; 100–115E)
CPN13	0.40	Fifth power of January temperature anomaly over (20–30N; 5–35E)
CPN14	0.38	January temperature anomaly over (20–35N; 30–10W)
CPN15	–0.37	Square of April temperature anomaly over (20–35N; 75–85E)
CPN16	–0.36	Fifth power of April sea-level pressure anomaly over (Equator – 20N; 0–30E)

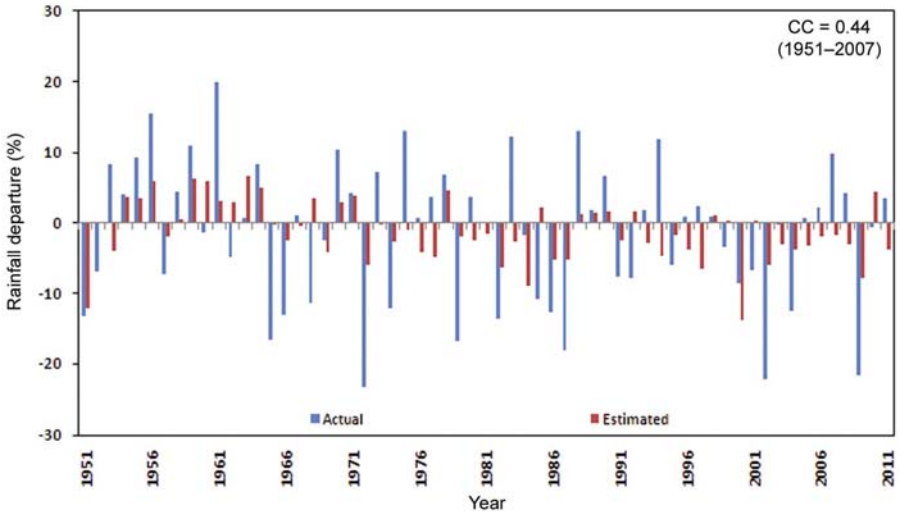

Figure 5. Actual and estimated ISMR using single multiple regression equation.

A multiple regression equation is formulated using CP1 and CP5 to predict ISMR.

Rainfall departure (%) = 0.82 – 3.37 (CP1) – 2.28 (CP5).

Multiple correlation coefficient (MCC) is 0.44. The observed and estimated seasonal rainfall departure (%) over India is depicted in Figure 5. This model predicts below-normal ISMR reasonably well. SLP over region-1 and region-5 in Figure 3 is a manifestations of SO and NAO respectively. Inclusion of these two cluster parameters (CP1 and CP5) in multiple regression equation suggests that other ST and SLP cluster parameters are linked with two large-scale oscillations NAO and SO. But evolution of NAO and SO from winter to spring is opposite during contrasting phases of ESI tendency[19]. Hence the

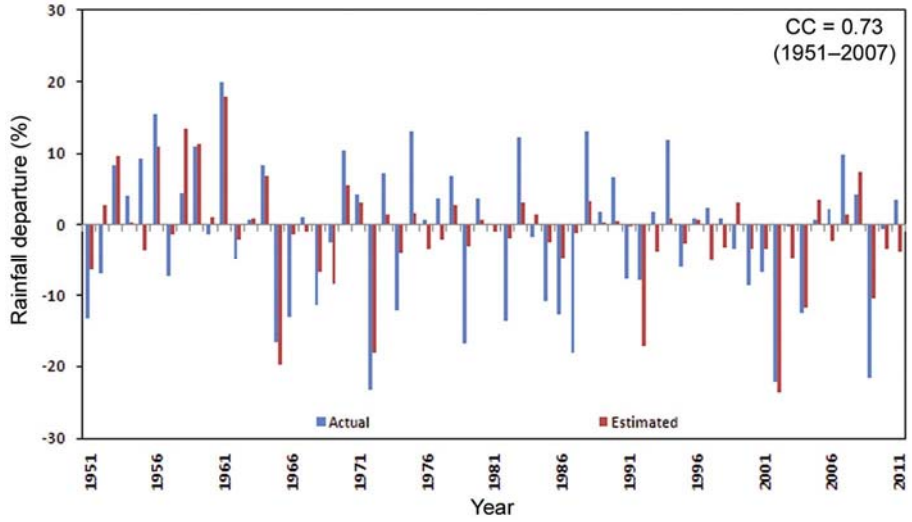

Figure 6. Actual and estimated ISMR departure (%) using two separate multiple equations for positive and negative phase of effective strength index tendency.

relationship between cluster parameters and ISMR may change during contrasting phases of ESI tendency.

During 1951–2007, 27 years show positive ESI tendency and 30 years show negative ESI tendency. ESI tendency indicates how the relative strength of the two oscillations NAO and SO is evolved from winter to spring and hence evolution of ST and SLP may change during contrasting phases of ESI tendency. Winter-time anomalous trough/ridge over the Eurasian region is indicated by the contrasting phases of ESI tendency[19]. Therefore, we take different parameters for predicting ISMR during contrasting phases of ESI tendency. CC between 62 cluster time-series and ISMR during contrasting phases of ESI tendency is computed. Table 2 describes three cluster parameters (CPP1, CPP2 and CPP3) showing significant association with ISMR during positive ESI tendency. CPP1 and CPP2 are mutually independent and the CC with ISMR during positive ESI tendency is –0.66 and –0.41 respectively. The locations of CPP1 and CPP2 are depicted in Figure 3 by region-6 and region-5 respectively. It reveals that during positive ESI tendency, SLP over North Atlantic Ocean is inversely associated with ISMR and the relationship is significant. A multiple regression equation for positive ESI tendency years is formulated using CPP1 and CPP2 to predict ISMR.

Rainfall departure (%)

$$= 1.18 - 1.46\,(\mathrm{CPP1}) - 2.4\,(\mathrm{CPP2}).$$

MCC is 0.70. Table 3 describes 16 cluster parameters (CPN1–CPN16) showing significant relationship with ISMR during negative ESI tendency. It shows large number of ST and SLP cluster parameters for predicting ISMR. The highest CC with ISMR is found by CPN1 (CC = –0.57) and its location is shown in Figure 3 by region-2. This region comprises of Nino region in the Pacific Ocean, which is known to affect ISMR inversely. Along with CPN1 two more independent cluster parameters, namely CPN9 and CPN15 show significant association with ISMR. Region-3 and region-4 in Figure 3 are the locations where CPN9 and CPN15 parameters are obtained respectively. Thus during contrasting phases of ESI tendency we have two different sets of cluster parameters. A multiple regression equation for negative ESI tendency years is formulated using CPN1, CPN9 and CPN15 to predict ISMR.

Rainfall departure (%)

$$= 6.64 - 36.04\,(\mathrm{CPN1}) - 4.85\,(\mathrm{CPN9}) - 6.7\,(\mathrm{CPN15}).$$

Multiple correlation coefficient = 0.70.

Thus during positive (negative) ESI tendency, winter SLP over North Atlantic (spring temperature over equatorial Pacific) shows highest association with ISMR. This may be because relative strength of NAO tendency (SO tendency) is more during positive (negative) ESI tendency. Figure 6 shows actual and estimated seasonal rainfall departure (%) using multiple regression equation depending on phase of ESI tendency. During 57 years from 1951 to 2007, out of 31 above-normal rainfall years only 22 years can be predicted as positive and out of 26 below-normal rainfall years 22 years can be predicted as negative. This model seems to predict ISMR better than the previous one (CC between actual and estimated = 0.73). The increase in MCC from 0.44 to 0.73 suggests that predictors should be selected depending upon the evolution of ST and SLP from January to April.

The SNN algorithm provides a homogeneous cluster of the parameters which can be used as predictors. ST and

SLP cluster parameters for predicting ISMR are different in contrasting phases of ESI tendency. During positive (negative) ESI tendency, only SLP (ST) cluster parameters are sufficient to predict ISMR. The skill in ISMR prediction can be improved using different prediction equations depending upon the phase of ESI tendency.

1. Gadgil, S. and Gadgil, S., The Indian monsoon, GDP and agriculture. *Econ. Polit. Wkly*, 2006, **XLI**, 4887–4895.
2. Verma, R. K., Subrmaniam, K. and Dugam, S. S., Interannual and long-term variability of the summer monsoon and its possible link with northern hemispheric surface air temperature. *Proc. Indian Acad. Sci.* (*Earth Planet. Sci.*), 1985, **94**, 187–198.
3. Mooley, D. A. and Paolino Jr, D. A., A predictive monsoon signal in the surface level thermal field over India. *Mon. Weather Rev*., 1988, **111**, 339–352.
4. Gowariker, V., Thapliyal, V., Kulshrestha, S. M., Mandal, G. S., Sen Roy, N. and Sikka, D. R., A power regression model for long range forecast of southwest monsoon rainfall over India. *Mausam*, 1991, **42**, 125–130.
5. Parthasarathy, B., Rupa Kumar, K. and Sontakke, N. A., Surface and upper air temperatures over India in relation to monsoon rainfall. *Theor. Appl. Climatol.*, 1990, **42**, 93–110.
6. Parthasarathy, B., Rupa Kumar, K. and Kothawale, D. R., Surface pressure and summer monsoon rainfall over India. *Adv. Atmos. Sci*., 1992, **9**, 359–366.
7. Krishna Kumar, K., Soman, M. K. and Rupa Kumar, K., Seasonal forecasting of Indian summer monsoon rainfall. *Weather*, 1995, **50**, 449–467.
8. Liu, X. and Yanai, M., Relationship between the Indian monsoon rainfall and the tropospheric temperature over the Eurasian continent. *Q. J. R. Meteorol. Soc*., 2001, **127**, 909–937.
9. Robinson, D. A., Bamzai, A. and Ramsay, B., Evaluating northern hemisphere snow cover during the satellite era: variations in extent and associations with temperature. In Proceedings of the 12th Symposium on Global Change and Climate Variations, American Meteorological Society, Albuquerque, NM, USA, 2001, pp. 36–39.
10. Ye, H. and Bao, Z., Lagged teleconnections between snow depth in northern Eurasia, rainfall in Southeast Asia and sea surface temperatures over the tropical Pacific Ocean. *Int. J. Climatol.*, 2001, **21**, 1607–1621.
11. Zhao, P. and Chen, L. X., Interannual variability of atmospheric heat source/sink over the Qinghai-Xizang (Tibetan) plateau and its relation to circulation. *Adv. Atmos. Sci.*, 2001, **18**, 106–116.
12. Rajeevan, M., Winter surface pressure anomalies over Eurasia and Indian summer monsoon. *Geophys. Res. Lett.*, 2002, **29**, 94-1–94-4.
13. Robock, A., Mu, M., Vinnikov, K. and Robinson, D., Land surface conditions over Eurasia and Indian summer monsoon rainfall. *J. Geophys. Res. D*, 2003, **108**, D4, 4131.
14. Sahai, A. K., Grimm, A. M., Satyan, V. and Pant, G. B., Long-lead prediction of Indian summer monsoon rainfall from global SST evolution. *Climate Dyn.*, 2003, **20**, 855–863.
15. Sahai, A. K., Chattopadhyay, R. and Goswami, B. N., SST based large multi-model ensemble forecasting system for Indian summer monsoon rainfall. *Geophys. Res. Lett.*, 2008, **35**, 1–9.
16. Ertoz, L., Steinbach, M. and Kumar, V., Finding clusters of different sizes, shapes, and densities in noisy, high dimensional data. In Proceedings of Third SIAM International Conference on Data Mining, San Francisco, USA, May 2003.
17. Boriah, S., Simon, G., Naorem, M., Steinbach, M., Kumar, V., Klooster S. and Potter, C., *Predicting Land Temperature Using Ocean Data*, KDD Seattle, WA, USA, 2004.
18. Kakade, S. B. and Kulkarni, A., Relationship between ESI tendency and Indian monsoon rainfall: a possible mechanism. *Atmos. Sci. Lett.*, 2012, **13**, 22–28.
19. Kakade, S. B. and Kulkarni, A., The changing relationship between surface temperatures and Indian monsoon rainfall with the phase of ESI tendency. *Adv. Meteorol.*, 2012, doi: 10.1155/2012/934624
20. Jarvis, R. A. and Patrick, E. A., Clustering using a similarity measure based on shared nearest neighbors. *IEEE Trans. Comput.*, 1973, **C-22**, 1025–1034.
21. Kripalani, R. H. and Kulkarni, A., Climatology and variability of historical Soviet snow depth data: some new perspectives in snow – Indian monsoon teleconnections. *Climate Dyn.*, 1999, **15**, 475–489.

ACKNOWLEDGEMENTS. We thank Prof. B. N. Goswami, Director, Indian Institute of Tropical Meteorology, Pune for providing the necessary facilities. We also thank the anonymous reviewers for providing useful suggestions that helped improve the manuscript.

Received 6 June 2013; revised accepted 30 August 2013

Plant height profiling in western India using LiDAR data

P. Tripathi* and M. D. Behera

Centre for Oceans, Rivers, Atmosphere and Land Sciences,
Indian Institute of Technology, Kharagpur 721 302, India

Plant height has always been a subject of research in forest and vegetation sciences. Space-borne LiDAR data of Geoscience Laser Altimeter System (GLAS) on the Ice, Cloud and land Elevation Satellite (ICESat) have opened up new possibilities to analyse vegetation height. Here, we have analysed the plant height panorama for various forest vegetation classes of western India and understood their profile in terms of topography, vegetation canopy density and presence of heterogeneous features within the LiDAR footprints. Of the total 14,230 LiDAR hits for western India falling in 32 forest vegetation classes, we eliminated extreme plant height ranges to retain 9553 (67.13%) data points for further analysis. Maximum number of data points was observed over temperate coniferous forest, pine forest and desert dune scrub with 2119, 936 and 1770 number of LiDAR hits respectively. The maximum and minimum plant height range varied between 70 and 2.2 m for temperate coniferous forest and alpine scrub. In general, we noticed inaccuracy in the plant height estimates from GLAS data points for higher slope and elevation. Overestimation in data points could be attributed to the presence of anthropogenic features, viz. buildings, settlement and

*For correspondence. (e-mail: tripathy.poonam@gmail.com)